Laser-induced decompression shock development in fused silica

Junlan Wang,[a] Richard L. Weaver, and Nancy R. Sottos
Department of Theoretical and Applied Mechanics, University of Illinois at Urbana-Champaign, 216 Talbot Lab, 104 S. Wright Street, Urbana, Illinois 61801

(Received 15 January 2003; accepted 20 March 2003)

Laser-induced weak shock formation in fused silica is studied using standard wave mechanics and applied to thin-film laser spallation experiments. Due to the negative nonlinear elasticity of fused silica, a laser-induced Gaussian stress pulse evolves into a shock after traveling a certain distance in a fused silica substrate. Experimental observations confirm theoretical predictions of shock development. A decompression shock forms and greatly enhances interfacial failure of a thin film deposited on the substrate. The effects of laser fluence and substrate thickness (attenuation) on shock development are also investigated. © *2003 American Institute of Physics.*
[DOI: 10.1063/1.1574175]

I. INTRODUCTION

Laser pulse absorption generates high amplitude, short duration stress wave pulses that can be used to load the interface between a film and a substrate. The subsequent failure of the film is then related to the known dynamic stress state thereby allowing the strength of the interface to be inferred. The laser spallation technique, introduced by Yang,[1] Vossen[2] and further developed by Gupta *et al.*[3–8] is shown schematically in Fig. 1. A high-energy laser pulse (duration of nanoseconds) from a Q-switched laser ($\lambda = 1064$ nm) impinges onto a thin metallic absorbing layer (AL) sandwiched between a thin confining layer (CL) and the back surface of the substrate (S). The energy-absorbing layer is chosen to be much thicker (typically 0.5 μm) than the critical penetration depth (on the order of tens of nm) of laser light at this wavelength. Under this consideration, it is assumed that the total laser energy is deposited at the interface of the confining layer and the absorbing layer. The sudden expansion of the confined layer generates a compressive stress wave of rise time comparable to the laser pulse that propagates towards the test film/substrate interface. Reflection of the compressive wave packet from the free surface of the test film creates a tensile pulse, which leads to spallation of the film. The fall time of the compressive stress profile generated in the substrate is a critical parameter governing film failure. The tensile stress developed at the interface is proportional to the time derivative of the substrate stress, hence a faster fall time enhances the ability to fail the film.

Theoretical analysis[9] reveals that the compressive stress pulse generated in the substrate is a copy of, and proportional to, the deposited laser pulse at the interface (i.e., a Gaussian laser pulse deposition results in a Gaussian stress pulse in the substrate). The amplitude of that stress is determined by the material properties of the two adjacent media. In many cases, the pulses that are generated have compressive stress amplitudes of the order of GPa, corresponding to strains $\epsilon_{\max}$ of the order of 1%. Such a pulse can be expected to evolve a weak shock in times proportional to the time scales of the laser pulse and inversely proportional to $\epsilon_{\max}$. The generation of a shock and in particular the precise time and distance also depend on the nonlinear parameters of the medium and on the competing effects of absorption and attenuation. Because the test film interface is loaded by the difference between the stress at one time and the stress at a time $2h/c$ earlier (due to reflection from the free surface) (where h is the film thickness, c is the longitudinal wave speed in film),[10] the development of a shock with an extremely rapid rise (or fall) time will significantly affect that load. The several-nanosecond rise time Gaussian pulse generated by the laser is inefficient for the purpose of spalling a 1 μm film. For such a film, the interface load is related to the pulse's stress change over a time difference of 0.33 ns (0.66 ns for shear waves). The stress difference on the interface is therefore substantially less than the peak stress developed in the Gaussian stress pulse. If a shock develops with a subnanosecond rise (or fall) time, the peak stress on the interface can approach the peak value in the pulse. Therefore, materials with nonlinear properties that enhance shock development are desirable for testing thin-film interface properties.

Because fused silica has the unusual property of softening under modest compression, the development of weak shocks in fused silica has received considerable attention in the literature. Wackerle[11] first reported the basic characteristics of compressive wave shapes in fused silica, including a ramp-wave front up to ~4 GPa (40 kbar). He concluded that fused silica behaves as a nonlinear elastic solid up to the phase change at 9.8 GPa. Later, Barker and Hollenbach[12] demonstrated the existence of rarefaction shocks in fused silica (as opposed to the more common compression shocks found in other materials). They refined Wackerle's compressive wave data in the low stress region and confirmed Wackerle's assertion of elasticity by determining that the release stress–strain path followed in a rarefaction wave coincided with the compressive stress–strain path, which determines the compressive wave shape. Barker and Hollenbach[12] also

[a]Author to whom correspondence should be addressed. Current address: Brown University, Box D, Division of Engineering, 184 Hope Street, Providence, RI 02912; electronic mail: junlan_wang@brown.edu.

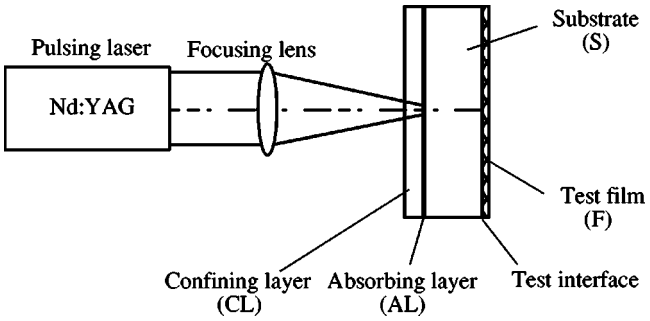

FIG. 1. Schematic of the tensile laser-spallation technique.

fitted the compressive wave data into a fourth-order stress–strain relation

$$\sigma=\alpha\epsilon+\beta\epsilon^2+\gamma\epsilon^3+\zeta\epsilon^4, \tag{1}$$

where σ is the stress in GPa, $\alpha=77.6$ GPa, $\beta=-415.9$ GPa, $\gamma=3034.0$ GPa and $\zeta=-6926.0$ GPa. Equation (1) is valid for stresses up to the phase transition at about 9.8 GPa. The stress–strain relation in Eq. (1) is plotted in Fig. 2(a) for stresses up to 9.8 GPa. By taking the derivative of Eq. (1) with respect to ϵ, one obtains the relation between the tangent modulus and stress (or strain), which is plotted in Fig. 2(b). Under compressive stress below 4 GPa (corresponding to a strain of 6.5%), the tangent modulus decreases or ''softens'' with increasing stress. For stresses above 4 GPa, the tangent modulus increases or ''hardens'' with increasing stress. In the low stress region, fused silica has the potential for developing a shock.

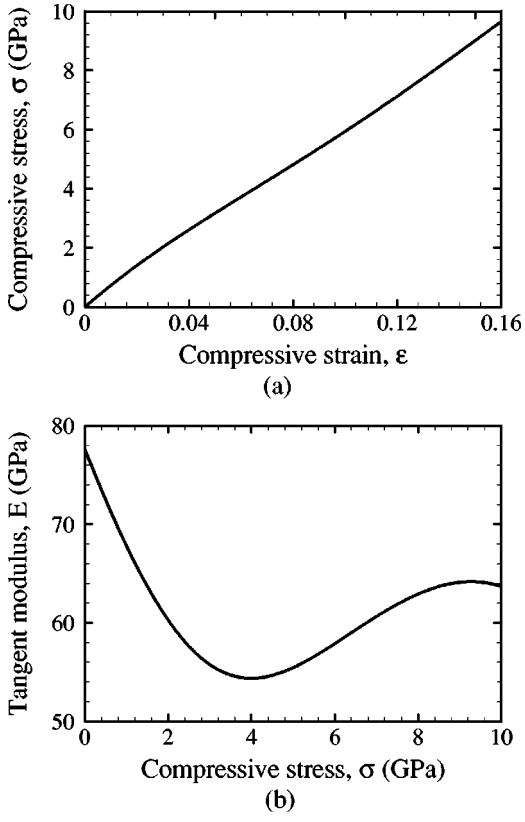

FIG. 2. Nonlinear elastic properties of fused silica: (a) stress–strain relation; (b) tangent modulus as a function of stress.

II. THEORETICAL ANALYSIS OF THE SHOCK DEVELOPMENT

Standard wave-propagation theory in nonlinear elastic solids[13] is used to analyze the shock development problem in fused silica. First, the wave motion is considered in the reference frame (X, t). The governing equations are

$$\rho_0\frac{\partial v}{\partial t}=\frac{\partial\sigma}{\partial X} \quad \text{(balance of momentum)}, \tag{2}$$

$$\frac{\partial\epsilon}{\partial t}=\frac{\partial v}{\partial X} \quad \text{(conservation of material)}, \tag{3}$$

where ρ_0 is the density, $v(X,t)$ and $\sigma(X,t)$ are the material velocity and stress, respectively. Assuming a constitutive relation of the form

$$\sigma=\sigma(\epsilon), \tag{4}$$

and that v is a single valued function of σ, one may write

$$\frac{\partial v}{\partial t}=\frac{\partial v}{\partial\sigma}\frac{\partial\sigma}{\partial t}, \quad \frac{\partial v}{\partial X}=\frac{\partial v}{\partial\sigma}\frac{\partial\sigma}{\partial X} \tag{5}$$

and Eqs. (2) and (3) become

$$\rho_0\frac{\partial v}{\partial\sigma}\frac{\partial\sigma}{\partial t}-\frac{\partial\sigma}{\partial X}=0, \tag{6}$$

$$\frac{\partial\epsilon}{\partial\sigma}\frac{\partial\sigma}{\partial t}-\frac{\partial v}{\partial\sigma}\frac{\partial\sigma}{\partial X}=0. \tag{7}$$

Solving Eqs. (6) and (7) leads to

$$\rho_0\left(\frac{\partial v}{\partial\sigma}\right)^2=\frac{\partial\epsilon}{\partial\sigma}. \tag{8}$$

For a given function of $\sigma(\epsilon)$, $\partial\epsilon/\partial\sigma$ is fixed function of σ; thus Eq. (8) has two solutions for $v=v(\sigma)$. Once the root is chosen, a speed of propagation of characteristics can be identified [from Eq. (6)]

$$c(\sigma)=\frac{1}{\rho_0\dfrac{\partial v}{\partial\sigma}}=\frac{1}{\sqrt{\rho_0\dfrac{\partial\epsilon}{\partial\sigma}}}=\sqrt{\frac{1}{\rho_0}\frac{\partial\sigma}{\partial\epsilon}}. \tag{9}$$

The time it takes the stress wave to propagate through a distance L is given by

$$t_L=\frac{L}{c(\sigma)}=\frac{L\sqrt{\rho_0}}{\sqrt{\dfrac{\partial\sigma}{\partial\epsilon}}}. \tag{10}$$

For a fused silica substrate with the stress–strain relation provided by Barker and Hollenbach[12] [Eqs. (9) (10)], the speed of the propagation of characteristics is

$$c(\sigma)=\sqrt{\frac{1}{\rho_0}(\alpha+2\beta\epsilon)} \quad \text{(second-order approximation)}$$

$$=\sqrt{\frac{\alpha}{\rho_0}\left(1+\frac{2\beta\sigma}{\alpha^2}\right)} \quad \text{(first-order approximation)}$$

$$=\sqrt{\frac{\alpha}{\rho_0}}\left(1+\frac{\beta\sigma}{\alpha^2}\right) \quad ((1+a)^{1/2}\approx 1+a/2)$$

$$=c_0\left(1+\frac{\beta\sigma}{\alpha^2}\right), \tag{11}$$

where $c_0=\sqrt{\alpha/\rho_0}$ coincides with the low-amplitude dilatational sound velocity in fused silica, 5.9391 mm/μs. The time/travel-distance ratio is given by

$$\frac{t_L}{L}=\frac{1}{c_0}\left(1-\frac{\beta\sigma}{\alpha^2}\right). \tag{12}$$

Equations (11) and (12) reveal that in the low stress region, the speed of the stress wave as well as the time/travel-distance ratio are linear functions of the compressive stress. Higher amplitude stress has a lower travel speed, and thus higher time/travel-distance value, i.e., the higher amplitude compressive stress travels slower. In the actual laser spallation experiments, the stress pulse generated at the absorbing layer interface is a compressive Gaussian stress pulse. When it travels through a fused silica substrate, the Gaussian stress pulse will be deformed according to the relation given in Eq. (12). The low stress at the front of the pulse travels most quickly. The peak stress, initially a few nanoseconds behind the front of the pulse, will be retarded relative to the front of the pulse. The rising part of the compression pulse will be stretched and eventually evolve into a linear ramp. The falling part of the stress pulse evolves in a very different manner. The tail of the initial pulse propagates more quickly than the peak. After certain time, the tail overtakes the peak and a discontinuity in stress (and therefore in material velocity) develops. The time it takes for the tail of the stress pulse to overtake the peak, t_{sh}, can be estimated using the material properties apparent in the slope of the ramp in Eq. (12), the fall time of the laser pulse T, and the peak stress of the Gaussian stress pulse σ_p as

$$t_{\mathrm{sh}}=\frac{T\alpha^2}{\beta\sigma_p}. \tag{13}$$

The deformed profile of an initial Gaussian stress pulse at any location x before it forms the shock is given by the stress–time of arrival relation

$$t=t_0+\frac{x}{c_0}\left(1-\frac{\beta\sigma}{\alpha^2}\right), \quad \text{for } x<c_0t_{\mathrm{sh}}, \tag{14}$$

where t_0 is related to stress σ by Eq. (15), i.e.

$$\sigma(t_0)=\sigma_{\max}\exp\left(-\frac{2t_0^2}{T^2}\right), \tag{15}$$

where $\sigma_{\max}$ is the peak compressive stress.

Equation (13) indicates that the time for a stress pulse to evolve into a shock is directly proportional to the fall time of the laser pulse and inversely proportional to the amplitude of the stress. The laser used in our experiments has a fixed fall time of 4.1 ns.[9] Thus, the higher the amplitude of the compressive stress, the shorter it takes the stress to evolve into a shock. From the values of T, α and β provided earlier, Eq. (13)'s estimated time for a shock to develop for a 1.0, 2.0, and 3.0 GPa stress pulse are 58, 28, and 19 ns, respectively. Figure 3 shows the evolution process of a 1.0, 2.0, and 3.0 GPa initial Gaussian stress pulse over time, calculated using Eqs. (14) and (15). A shock is developed for all three stress pulses at times similar to those estimated in Eq. (13). Clearly, stress pulses with higher peak values develop a shock in a shorter time.

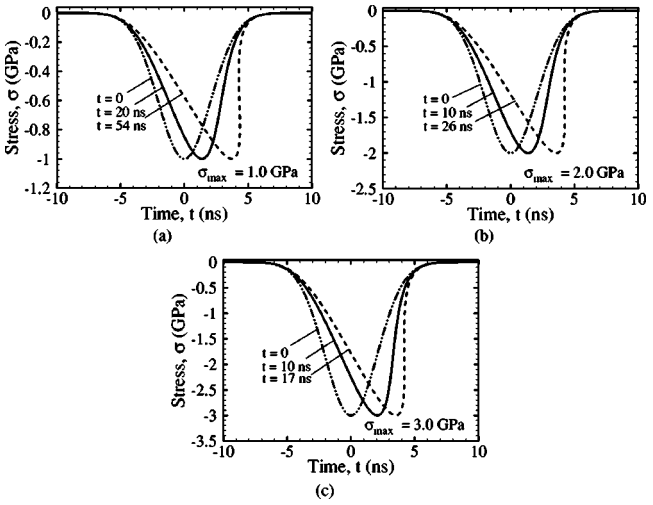

FIG. 3. Evolution of the Gaussian stress pulse in fused silica with time: (a) 1.0 GPa peak stress; (b) 2.0 GPa peak stress; (c) 3.0 GPa peak stress.

In Fig. 4, the initial Gaussian stress pulses with peak values of 1.0, 2.0, and 3.0 GPa are plotted together in (a), and the deformed stress pulses after traveling 20 ns in the media are plotted in (b). The peak stresses from the three pulses are fitted into a linear equation. The slope of the linear fit, -0.724 GPa/ns, is exactly predicted from Eq. (12).

After the shock is formed, the stress profile will continue to evolve according to the equal-area rule.[14] The evolution process can be explained using the simplified model shown in Fig. 5. The total area under the stress profile is A_0, the duration of the ramp is D, and the peak stress at an arbitrary moment is σ_p. Once a discontinuity has developed at the trailing edge of the profile, it will move with the speed equal to the average of the wave speeds behind and ahead of the shock[13]

$$v_{\mathrm{sh}}=\frac{v_{\mathrm{sh}+}+v_{\mathrm{sh}-}}{2}=c_0\left(1+\frac{\beta\sigma_p}{2\alpha^2}\right). \tag{16}$$

Thus, the shock will move more slowly than the front of the linear ramp (zero stress). The ramp part will continue to be stretched and D will increase with time. According to the equal-area rule, the area A_0 will remain constant and thus

$$D=\frac{2A_0}{\sigma_p}, \tag{17}$$

$$\frac{\partial D}{\partial t}=-\frac{c_0\beta\sigma_p}{2\alpha^2}. \tag{18}$$

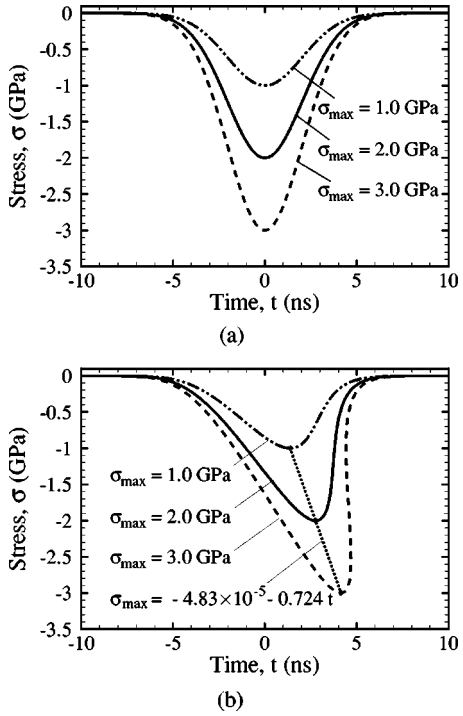

FIG. 4. Evolution of the Gaussian stress pulse in fused silica with time: (a) the initial Gaussian stress pulse of 1.0, 2.0, 3.0 GPa peak value; (b) the stress pulse in (a) traveled 20 ns in the substrate.

Substituting Eq. (17) into Eq. (18), one obtains

$$\frac{\partial \sigma_p}{\partial t} = \frac{c_0 \beta}{4A_0 \alpha^2} \sigma^3. \tag{19}$$

The solution of Eq. (19) takes the form

$$\sigma_p = \frac{1}{\sqrt{C_0 - \dfrac{c_0 \beta}{2A_0 \alpha^2} t}}, \tag{20}$$

where C_0 is a constant. Application of the initial condition

$$\sigma_p = \sigma_{p0} \quad \text{at } t = t_{\text{sh}}, \tag{21}$$

where σ_{p0} is the peak stress at the time the shock forms, yields

$$C_0 = \sigma_{p0}^{-2} + \frac{c_0 \beta}{2A_0 \alpha^2} t_{\text{sh}}. \tag{22}$$

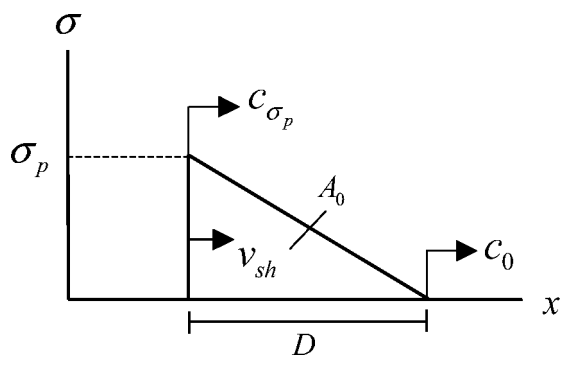

FIG. 5. Schematic of the shock motion.

Substituting the value of C_0 into Eq. (20) and simplifying, one obtains

$$\sigma_p = \frac{\sigma_{p0}}{\sqrt{1 - \dfrac{c_0 \beta}{2A_0 \alpha^2}(t - t_{\text{sh}})\sigma_{p0}^2}}. \tag{23}$$

Therefore

$$A_0 = \tfrac{1}{2} D \sigma_{p0} \approx \tfrac{1}{2}(2c_0 T)\sigma_{p0} = c_0 T \sigma_{p0}. \tag{24}$$

Substituting Eqs. (24) and (13) into Eq. (23), one finally obtains

$$\sigma_p = \frac{\sigma_{p0}}{\sqrt{3/2 - \dfrac{\beta \sigma_{p0}}{2T\alpha^2} t}}, \quad \text{for } t > t_{\text{sh}}. \tag{25}$$

For fixed substrate thickness L

$$\sigma_p = \frac{\sigma_{p0}}{\sqrt{3/2 - \dfrac{\beta \sigma_{p0} L}{2c_0 T \alpha^2}}}. \tag{26}$$

The above equation is valid only after the shock has formed. In order to guarantee shock development before the stress travels through distance L, σ_{p0} must satisfy

$$\sigma_{p0} \geqslant \sigma_{p0}^{\min} = \frac{c_0 T \alpha^2}{\beta L}. \tag{27}$$

For a 1.5-mm-thick fused silica substrate the minimum peak stress is, $\sigma_{p0}^{\min} = 0.234$ GPa and for a 3-mm-thick fused silica substrate, $\sigma_{p0}^{\min} = 0.116$ GPa. In Fig. 6, the values of the attenuation factor σ_p / σ_{p0} and σ_p are plotted as functions of σ_{p0} for two substrate thicknesses, 1.5 and 3 mm, respectively.

As expected from Eq. (26) for the same initial peak stress σ_{p0}, greater attenuation occurs in the thicker substrate. For the same substrate thickness, L, greater attenuation occurs for larger initial peak stress σ_{p0}. The remaining peak stress σ_p, however, is still greater for greater initial peak stress σ_{p0} because $\sigma_p \propto (\sigma_{p0})^{1/2}$, for large σ_{p0}.

III. EXPERIMENTAL VERIFICATION

A. Procedure and sample preparation

Laser-induced shock development in fused silica was investigated using the spallation experiment described previously (Fig. 1). Samples consisted of a fused silica substrate with a thin aluminum test film and absorbing layer evaporated onto either side. Two different substrate thicknesses, 1.5 and 3.0 mm were tested. The Al deposition rate was held between 10 and 15 Å/s and the bell jar controlled at 2–5 mTorr. The test film thickness ranged from 0.5 to 1.1 μm depending on the substrate thickness. The optimal absorbing layer thickness was 0.4 μm for all samples.[10] Waterglass was chosen for the confining layer based on previous research.[7,10] The thickness of the waterglass layer significantly affected stress wave generation. As a result, waterglass thickness was varied between 0.4 and 30 μm depending on the substrate

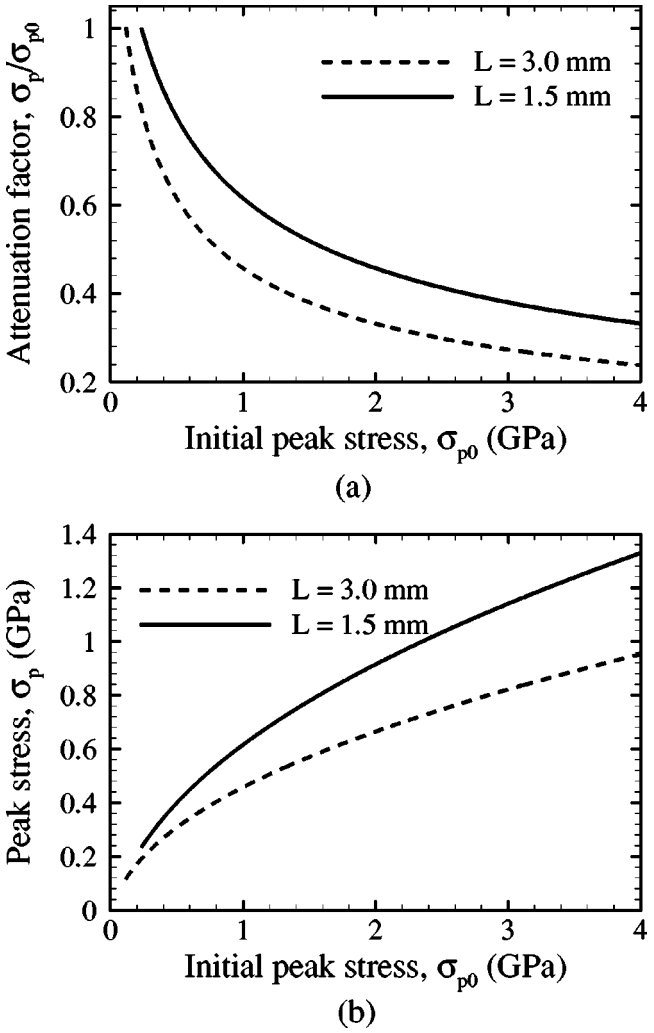

FIG. 6. Shock attenuation in fused silica: (a) attenuation factor as a function of initial peak stress and substrate thickness; (b) remaining peak stress as a function of initial peak stress and substrate thickness.

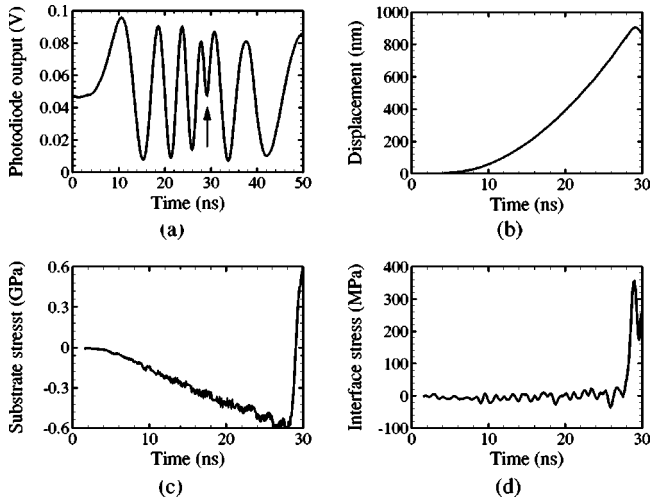

FIG. 7. Typical data profile for a 1.0-μm-thick Al film deposited on a 3000-μm-thick fused silica substrate (laser fluence of 0.140 J/mm^2): (a) interferometric fringe pattern, arrow points to turning point; (b) displacement profile; (c) substrate stress profile; (d) interface stress profile.

thicknesses. For thick waterglass layers (above 8 μm), waterglass solution was applied to the sample with a swab. For thinner layers, a standard photolithography spinner (Headway Research Inc., Garland, TX) was required. The final layer thickness was governed by the spinner rpm and the viscosity of the waterglass solution. The viscosity of the solution was adjusted by diluting the as received waterglass.

Samples were tested with an infrared, Nd:YAG (yttrium-aluminum-garnet)laser pulse ($\lambda = 1064$ nm) with a variable energy content between 1 and 110 mJ and a rise time on the order of 5 ns. The nominal diameter of the YAG laser beam was 3.5 mm. This beam was focused to a 1-mm-diam spot on the absorbing layer. (The theoretical analysis of Sec. II modeled the wave propagation as essentially one dimensional. This is justified for sufficiently short acoustic wavelength λ, or large diameter source or short propagation distance. One may invoke the usual acoustician's rule that the near field extends from a piston source of diameter D a distance $D^2/4\lambda$. Taking D to be 1 mm and λ to be 60 μm (corresponding to the nominal wavelength of the initially generated compressive pulse) one finds that the center of the beam remains plane-wave like for a propagation distance of 4 mm, greater than the thickest substrate used in the current experiment. If the appropriate λ is that of the shock, this distance is even greater.) By controlling the laser fluence, stress waves were generated with sufficient amplitude to fail the film/substrate interface. The out-of-plane displacement at the test film surface was measured with a Michelson interferometer.

From displacement measurements at the free surface, the stress history at the interface is inferred using standard wave mechanics[15] and the maximum stress acting on the interface calculated. Details of the interferometric displacement measurement are provided in Wang, Weaver, and Sottos.[10] Once the free surface displacement, u, is obtained, the compressive stress propagating from the absorbing layer towards the substrate is calculated using simple one-dimensional wave mechanics

$$\sigma_{\text{sub}} = -\frac{1}{2}(\rho c)_{\text{sub}}\frac{\partial u}{\partial t}. \tag{28}$$

For small film thickness h, the interface stress is calculated using

$$\sigma_{\text{inter}} = -(\rho h)_{\text{film}}\frac{\partial^2 u}{\partial t^2}. \tag{29}$$

B. Experimental results

A typical interferometric signal measured for a 1.0-μm-thick Al film deposited on a 3000-μm-thick fused silica substrate is shown in Fig. 7(a). The fringes develop over 20–30 ns and become more tightly spaced with time, indicating acceleration. At 29 ns, a turning point occurs (marked by an arrow) where the material velocity changes direction in the middle of a fringe. The displacement profile of the film free surface [Fig. 7(b)] is calculated from the fringe data [Fig. 7(a)]. Each full fringe corresponds to half wavelength ($\lambda/2 = 257$ nm) out-of-plane displacement. The compressive sub-

strate stress [Fig. 7(c)] and the stress at the test film interface after reflecting from the free surface [Fig. 7(d)] are calculated from Eqs. (28) and (29), respectively.

As expected from previous shock analysis, the initial Gaussian stress pulse evolves into a decompression shock long before it reaches the test film. The rising part of the initial compression pulse thus evolves into a linear ramp, a classic acceleration wave. This ramp is precisely what is seen in Fig. 7(c). The slope of that ramp (in units of stress per time/thickness) is a material parameter and is the same as that reported by Barker and Hollenbach.[12] The falling part of the stress pulse evolves in a very different manner. The tail of the initial pulse propagates more quickly than does the peak. It overtakes the peak in a time which can be calculated using Eq. (13). A discontinuity in stress (and therefore also in material velocity) develops when the tail overtakes the peak. That sufficient time has occurred in the present case for a decompression shock to develop is evident. After traveling through the substrate, the rising front edge of the pulse has stretched from about 4.1 to 20 or 30 ns. The falling tail end of the pulse has compressed by the same amount. An initial fall time of a few nanoseconds has therefore been reduced to nearly zero and this occurs long before the pulse arrives at the test film.

The experimental picture is complicated somewhat by the presence of a tensile wave, reflected from the back of the confining layer. The surface properties of that confining layer are not well controlled. Assuming a plausible longitudinal wave speed in the confining layer, the original compressive pulse is followed, about 30 ns later, by a tensile pulse of comparable magnitude. Being tensile, it propagates faster than the peak compressive stress, and faster than the low stress tail of the main pulse. It eventually overtakes the compressive pulse. In Fig. 7, the shock is followed by a regime in which the velocity has changed sign indicating that the tensile pulse has overtaken the compression pulse.

To verify the effect of the initial peak stress, different laser fluences were deposited onto different spots to generate stress pulses with different amplitudes. The sample has a test film thickness of 1.1 μm, fused-silica substrate thickness of 3000 μm, absorbing layer thickness of 0.4 μm and confining layer thickness of $\sim 20\ \mu$m. The YAG laser fluence was stepped from 0.056 to 0.140 J/mm^2 as the YAG laser was moved to different positions on the sample. Figure 8 shows the development of stress with increasing laser fluence. As laser fluence increases, the maximum compressive substrate stress also increases. At 0.056 J/mm^2 laser fluence, the maximum substrate stress of 0.28 GPa is achieved in a rise time of 18 ns; while for 0.140 J/mm^2 laser fluence a maximum substrate stress of 0.6 GPa is obtained in 28.5 ns. The higher maximum stress always occurs at later times and is approximately proportional to the laser fluence. The shock profiles in Fig. 8 are consistent with the nonlinear behavior of fused silica. The slope of the ramp is fitted by a linear function. The average slope of the stress ramps, -0.026 GPa/ns, is close to the theoretical value, -0.028 GPa/ns, obtained using Barker's material parameters.[12] From these stress profiles, an effective wave speed can be extracted as a function

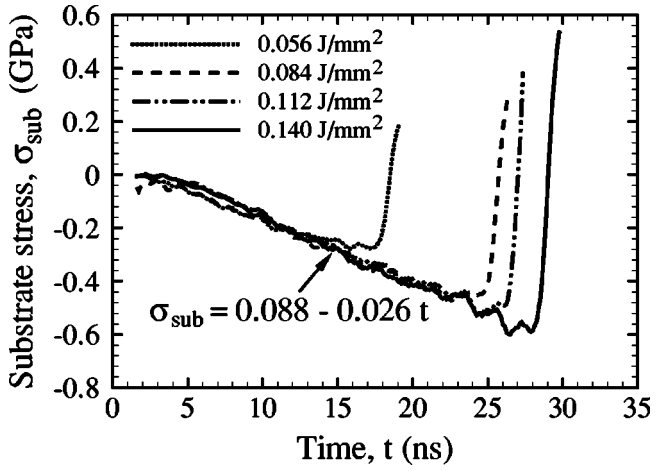

FIG. 8. Effect of laser fluence for a 1.1-μm-thick aluminum film deposited on a 3000-μm-thick fused silica substrate with 0.4-μm-thick absorbing layer.

of stress. The higher compressive stresses arrive later because higher compression means slower waves.

Experiments were also carried out on a thinner substrate. Typical interferometric data obtained on a 0.5-μm-thick Al film deposited on a 1500-μm-thick fused silica substrate with a 0.4-μm-thick waterglass confining layer are shown in Fig. 9. Similar to the data shown in Fig. 7, the fringe spacing decreases just before 22 ns where a sharp turning point occurs in the middle of a fringe. As a result, a linear ramp is formed in the substrate stress followed by a sharp shock. Since the shock only traveled half of the distance as the shock in Fig. 7, less attenuation results in a much higher compressive peak stress of about 1.2 GPa in the substrate and a very high tensile stress of about 420 MPa at the film interface. Thus the development of the shock significantly enhances the interface failure, especially for a very thin film or a thick substrate.

Experiments on both 3000 and 1500 μm reveal that waterglass confining layer thickness influences the measured shock stress profiles possibly through affecting the amplitude of the generated Gaussian stress pulse. Typical interferometric data obtained on a 0.5 μm Al film on a 1500-μm-thick fused silica substrate with a slightly thinner waterglass confining layer thickness, 0.25 μm, are shown in Fig. 10. Fewer fringes were developed before the turning point and a much lower substrate stress, only about 0.52 GPa, is generated. Thus thinner waterglass results in lower substrate stress, and also less film damage.

A series of experiments done with different waterglass thickness on the two substrate thicknesses, 3000 and 1500 μm indicated that different substrate thickness requires different optimum waterglass thickness to generate enough stress to fail the interface. The optimum thickness for the 1500-μm-thick fused silica is about 0.4 μm and the optimum waterglass thickness for 3000-μm-thick fused silica is above 8 μm. The exact thickness is hard to determine due to the difficulty in accurately controlling the waterglass thickness above 8 μm, but is approximately 30 μm.[9] A waterglass layer below the optimum thickness will not generate a stress high enough to fail the film and a waterglass layer much

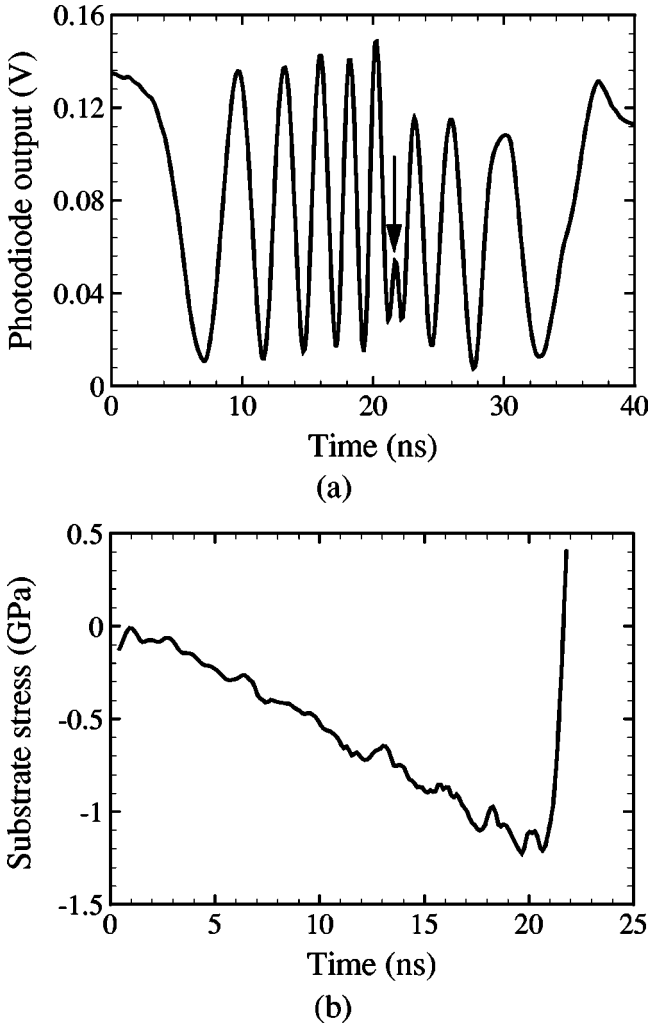

FIG. 9. Interferometric signal obtained for a 0.5-μm-thick aluminum film deposited on a 1500-μm-thick fused-silica substrate with 0.4-μm-thick waterglass (laser fluence of 0.140 J/mm^2): (a) photodiode output; (b) substrate stress. Arrow points to the position where fringes suddenly changed direction.

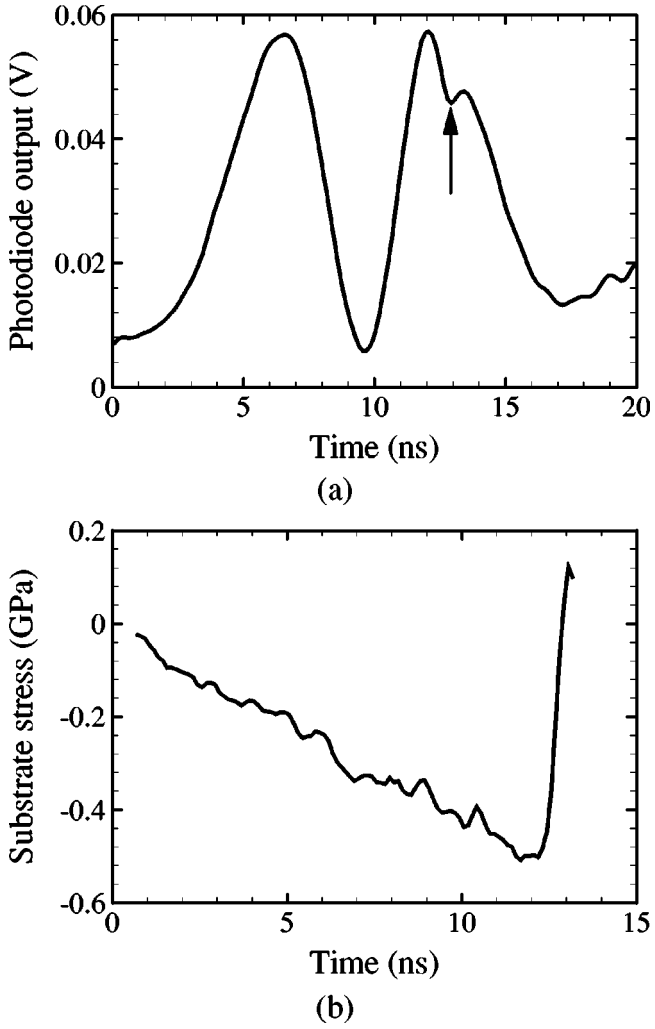

FIG. 10. Interferometric signal obtained for a 0.5-μm-thick aluminum film deposited on a 1500-μm-thick fused-silica substrate with 0.25-μm-thick waterglass (laser fluence of 0.140 J/mm^2): (a) photodiode output; (b) substrate stress. Arrow points to the position where fringes suddenly changed direction.

thicker than the optimum thickness tends to generate a very high stress level, resulting in excessive film failure. Thus, substrate thickness, film thickness, waterglass thickness and the laser fluence need to be carefully coordinated to optimize interfacial failure.

IV. CONCLUSIONS

Weak shock development following the deposition of a Gaussian laser pulse in fused silica was analyzed using standard wave mechanics and verified experimentally in a spallation test. Using the well documented negative nonlinear elastic properties of fused silica, theoretical predictions revealed that a decompression shock formed in time directly proportional to the rise time and inversely proportional to the peak value of the initial pulse. Evolution of the shock followed the equal-area rule and thus the peak stress attenuated as it traveled through a longer distance.

Experimental measurements confirmed theoretical considerations. A decompression shock was clearly evident in the interferometric data obtained during a tensile spallation experiment. The slope of the characteristic stress ramp was identical to the value for fused silica reported by Barker and Hollenbach[12] from early flyer plate experiments. The maximum stress developed in the substrate increased nonlinearly with laser power and decreased significantly with substrate thickness due to attenuation. The waterglass confining layer was also shown to play an important role in the shock formation. A thicker confining layer helped to generate a higher compressive stress in the substrate, but if the confining layer was too thick excessive film damage occurred. In all of the experiments, the fast fall time of the shock wave resulted in significant tensile loading of the planar interface between the substrate and the test film.

The development of the shock greatly enhances the ability to fail the interface, even at moderate laser fluences. This technique of laser-induced shock wave loading holds significant promise for testing interface properties of ultrathin films (below 100 nm) that are difficult to fail due to their small mass [see Eq. (29)].

ACKNOWLEDGMENTS

The authors gratefully acknowledge the support of the National Science Foundation (CMS-99-88127) and the University of Illinois Research Board. The authors would also like to acknowledge the use of the Frederick Seitz Materials Research Lab facilities and the Beckman Institute facilities at the University of Illinois.

[1] L. C. Yang, J. Appl. Phys. **45**, 2602 (1974).
[2] J. L. Vossen, *Adhesion Measurement of Thin Films, Thick Films and Bulk Coatings* (American Society for Testing and Materials, Philadelphia, 1978), Vol. 640, pp. 122, 123.
[3] V. Gupta, A. S. Argon, J. A. Cornie, and D. M. Parks, Mater. Sci. Eng., A **125**, 105 (1990).
[4] V. Gupta, A. S. Argon, D. M. Parks, and J. A. Cornie, J. Mech. Phys. Solids **40**, 141 (1992).
[5] V. Gupta and J. Yuan, J. Appl. Phys. **74**, 2397 (1993).
[6] J. Yuan and V. Gupta, J. Appl. Phys. **74**, 2388 (1993).
[7] V. Gupta, J. Yuan, and A. Pronin, J. Adhes. Sci. Technol. **8**, 713 (1994).
[8] J. Yuan, V. Gupta, and A. Pronin, J. Appl. Phys. **74**, 2405 (1993).
[9] J. Wang, Ph.D. thesis, University of Illinois, 2002.
[10] J. Wang, R. L. Weaver, and N. R. Sottos, Exp. Mech. **42**, 74 (2002).
[11] J. Wackerle, J. Appl. Phys. **33**, 922 (1962).
[12] L. M. Barker and R. E. Hollenbach, J. Appl. Phys. **41**, 4208 (1970).
[13] J. D. Achenbach, *Wave Propagation in Elastic Solids*, 4th ed. (North-Holland, Amsterdam, 1984).
[14] A. Pierce, *Acoustics* (McGraw–Hill, New York, 1981).
[15] J. Miklowitz, *Elastic Waves and Waveguides* (North-Holland, Amsterdam, 1978).